HHS Public Access

Author manuscript

Dent Mater. Author manuscript; available in PMC 2021 July 01.

Published in final edited form as:

Dent Mater. 2020 July ; 36(7): 865–883. doi:10.1016/j.dental.2020.04.008.

Bioactive amorphous magnesium phosphate-polyetheretherketone composite filaments for 3D printing

Prabaha Sikder[a], **Jessica A. Ferreira**[b], **Ehsan Akbari Fakhrabadi**[c], **Karla Z. Kantorski**[b,d], **Matthew W. Liberatore**[c], **Marco C. Bottino**[b,*], **Sarit B. Bhaduri**[a,e,*]

[a]Department of Mechanical, Industrial and Manufacturing Engineering, University of Toledo, Toledo, OH 43606, USA.

[b]Department of Cariology, Restorative Sciences, Endodontics, School of Dentistry, University of Michigan, Ann Arbor, MI 48109, USA.

[c]Department of Chemical Engineering, University of Toledo, Toledo, OH 43606, USA.

[d]Post-Graduate Program in Oral Science (Periodontology Unit), School of Dentistry, Federal University of Santa Maria, Santa Maria, Rio Grande do Sul, Brazil.

[e]EEC Division, Directorate of Engineering, The National Science Foundation, Alexandria, VA 22314, USA.

Abstract

Objectives: The aim of this study was to develop bioactive and osseointegrable polyetheretherketone (PEEK)-based composite filaments melt-blended with novel amorphous magnesium phosphate (AMP) particles for 3D printing of dental and orthopedic implants.

Materials and Methods: A series of materials and biological analyses of AMP-PEEK were performed. Thermal stability, thermogravimetric and differential scanning calorimetry curves of as-synthesized AMP were measured. Complex viscosity, elastic modulus and viscous modulus were determined using a rotational rheometer. *In vitro* bioactivity was analyzed using SBF immersion method. SEM, EDS and XRD were used to study the apatite-forming ability of the AMP-PEEK filaments. Mouse pre-osteoblasts (MC3T3-E1) were cultured and analyzed for cell viability, proliferation and gene expression. For *in vivo* analyses, bare PEEK was used as the control and 15AMP-PEEK was chosen based on its *in vitro* cell-related results. After 4 or 12 weeks, animals were euthanized, and the femurs were collected for micro-computed tomography (μ-CT) and histology.

[*]**Co-corresponding authors:Marco C. Bottino, DDS, MSc, PhD, FADM,** University of Michigan School of Dentistry, Department of Cariology, Restorative Sciences and Endodontics 1011 N. University (Room 5223), Ann Arbor, MI - 48109, USA. Tel: +1-734.763.2206 Fax: +1-734.936.1597. mbottino@umich.edu, **Sarit B. Bhaduri, PhD,** The University of Toledo, College of Engineering, Department of Mechanical, Industrial and Manufacturing Engineering Nitschke Hall 4029, 2801 W. Bancroft Street (MS#312), Toledo, OH - 43606, USA. Tel: + 1-419.530.8223 Fax: + 1-419.530.8206 Sarit.Bhaduri@utoledo.edu / sbhaduri@nsf.gov.

Data Availability

The raw/processed data required to reproduce these findings cannot be shared at this time as the data also forms part of an ongoing study.

Results: The collected findings confirmed the homogeneous dispersion of AMP particles within the PEEK matrix with no phase degradation. Rheological studies demonstrated that AMP-PEEK composites are good candidates for 3D printing by exhibiting high zero-shear and low infinite-shear viscosities. *In vitro* results revealed enhanced bioactivity and superior pre-osteoblast cell function in the case of AMP-PEEK composites as compared to bare PEEK. *In vivo* analyses further corroborated the enhanced osseointegration capacity for AMP-PEEK implants.

Significance: Collectively, the present investigation demonstrated that AMP-PEEK composite filaments can serve as feedstock for 3D printing of orthopedic and dental implants due to enhanced bioactivity and osseointegration capacity.

Keywords

Polyetheretherketone; amorphous magnesium phosphate; 3D printing; implants; osseointegration

1. Introduction

Orthopedic maladies, including but not limited to fractures, represent one of the most significant segments of global medical needs placing an economic burden on the healthcare system. In order to mitigate this issue, orthopedic biomaterials continue to be developed and refined based on patient-specific needs. As an example, polyetheretherketone (PEEK), a member of the polyaryl-ether-ketone family, has emerged as the leading high-performance thermoplastic candidate for replacing metallic implants [1]. The present investigation represents the initial step in our long-term effort in developing patient-specific implants, made from PEEK composites. There are two motivating reasons. First, by tailoring the Young's modulus of filled PEEK with that of cortical bone (18 GPa) PEEK-based implants can be made less prone to stress shielding, a well-known phenomenon that may ultimately lead to bone-implant debonding [2]. Second, PEEK is biocompatible, causes neither mutagenic effects nor significant inflammation, and can be radiation sterilized. These are the reasons why, according to the literature, there is a growing interest in utilizing PEEK in oral implantology [3]. Unfortunately, as compared to metallic implants, the major drawback of PEEK is its lack of osseointegration ability [4, 5].

Extensive research has been done to enhance the bioactivity of polymeric biomaterials including PEEK [6–11]. To that end, the development of various calcium phosphate (CaP) coatings have been reported [8, 12]. With the saturation of research on CaPs, there is a great deal of interest in alternate phosphates such as novel MgP compounds. A state-of-the-art review from our group explains the advantages of MgP [13] Noteworthy, our group recently demonstrated the synthesis of multi-functional bioactive MgP coatings on PEEK [14–18]. Broadly speaking, the reason for the reported favorable results is that magnesium ions (Mg^{2+}) are the fourth most abundant ion in mammals and participate in various cellular functions. For example, it is well-known that doping of Mg^{2+} in CaPs enhances osteogenic proliferation and differentiation [19, 20]. However, the present work expands the research beyond crystalline MgPs to amorphous phases [21]. It is known that amorphous calcium phosphate (ACP) has the tendency to crystallize [21]. Incorporation of Mg^{2+} ions in ACP inhibits crystallization [22, 23]. From that perspective, amorphous magnesium phosphate

(AMP) is more stable in that phase and is gaining increased attention as a member of the range of MgP compounds.

Alternatively, attempts have been made to incorporate bioceramic particles within a polymeric matrix to enhance implant osseointegration [24, 25]. Several *in vitro* [26, 27] and *in vivo* studies [28, 29] of bioactive PEEK composites containing CaP particles were reported. Of note, micro- [30] or nano-hydroxyapatite (HA) [31] in the shape of spheroids [28] or whisker [32], and β-tricalcium phosphate (β-TCP) [33] have been used as bioactive second phases in PEEK. However, none of the previously reported studies used amorphous CaP or MgP, thus warranting further investigation. A processing-related disadvantage is that PEEK possesses higher melting point than conventional polymers. This is the reason why many PEEK composites have been fabricated by the powder route and not via polymer processing. As a result, composites needed further processing to achieve desired shapes, if at all possible. It is an acknowledged fact that powder consolidation technique is not so convenient from the perspective of 3D printing.

Here, to the best of our knowledge, we present the first comprehensive investigation aiming at the development of bioactive amorphous magnesium phosphate-polyetheretherketone (AMP-PEEK) composite filaments (figure 1). These filaments will serve as feedstocks for three-dimensional (3D) printing in a subsequent effort. Our long-term goal is to fabricate bioactive, complex, defect-specific AMP-PEEK-based orthopedic and dental implants implants via 3D printing. Recently, we were successful in developing custom-designed PEEK based orthopedic implants via 3D printing and explored the pre-osteoblast behavior with them [34]. However, before going ahead and printing AMP-PEEK structures, it is important to analyze the overall properties of the AMP-PEEK filaments by itself and determine the most suitable composition for 3D printing. Hence, the sole purpose of this study was to explore the development of AMP-PEEK composite filaments and evaluate their properties comprehensively. A key aspect was to determine whether AMP particles can be homogeneously distributed in PEEK matrix, and without any matrix degradation. In this context, composite filaments were formed out of PEEK and with varying AMP contents via melt-blending followed by a series of comprehensive physical, thermal, rheological, and biological evaluations. In detail, the *in vitro* cellular responses, including the metabolic activities of the proliferated mouse pre-osteoblasts, their differentiation ability, and expression of the osteogenic genes were determined. Moreover, histological and micro-computed tomography analyses were performed using a rat femur model of bone-implant osseointegration.

2. Materials and Methods

2.1. Materials

AMP synthesis was carried out in-house, following the ethanol-assisted precipitation method [35] previously employed by Babaie et al. [36]. In brief, 11.52 g of magnesium nitrate hexahydrate ($Mg(NO_3)_2.6H_2O$), 98% purity, Alfa Aesar, Tewksbury, MA, USA) was added to 100 ml of water and 100 ml of ethanol followed by proper stirring. This solution was then added rapidly, at 37°C under constant stirring, to a solution containing 2.97 g of diammonium hydrogen phosphate ($(NH_4)_2HPO_4$, 99% purity, Fisher Scientific, Hampton,

NH, USA) in 250 ml water, 45 ml ammonia (11M) and 295 ml ethanol. The procedure resulted in the formation of precipitate which were collected, centrifuged and washed in ethanol. All the aforementioned steps were carried out within 15 min. Finally, precipitates were placed in an air-drying oven at 60°C overnight to form fine powders. PEEK powder (particle size ca. 80 μm) was procured from GoodFellow (Goodfellow Cambridge Limited, Cambridge Science Park, Cambridge, England) and used without any further processing.

2.2. AMP-PEEK blending

Different compositions of as-synthesized AMP and PEEK powders were first mixed using a 100W overhead stirrer (Mophorn, Huaian City, Jiangsu Province, China) for 3–6 min at room temperature. Table 1 contains the specimens' code and their respective compositions. To obtain well-mixed AMP-PEEK composites, melt-blending was carried out using the twin-screw extrusion method. Briefly, blended powders of appropriate AMP-PEEK compositions were fed into a twin-screw extruder (Xplore MC5, Xplore Instrument BV, Geleen, Netherlands) in 3 g batches. The co-rotating screws had a length of 150 mm each, and a fixed rotational screw speed of 50 rpm was chosen. Residence time was varied depending on the AMP content (table 1). Four different extrusion temperatures, namely 360°C, 370°C, 380°C and 400°C were chosen to investigate the effect of processing temperature on the composites. The extruded filaments ($(\phi = 2\text{mm}) = 2$ mm) were air-quenched and subsequently pelletized. For physicochemical and *in vitro* characterizations, specimen dimensions were 2 mm in diameter and 5 mm in length.

2.3. Physico-chemical characterizations

To analyze the thermal stability of AMP, the as-synthesized precipitates were heat-treated at 400°C, 500°C, 600°C and 800°C in an air-furnace oven. The effect of heat treatment on AMP was determined using focused beam mono-chromated CuKα radiation (44 kV, 40 mA) X-ray diffraction (XRD, Ultima III, Rigaku, Tokyo, Japan) for phase analyses and scanning electron microscopy (SEM, S4800, Hitachi, Tokyo, Japan) for morphological characteristics. A gas displacement pycnometer (AccuPyc 1330, MicroMeritics, Norcross, GA, USA) was used to measure the density of the AMP-PEEK composites. Theoretical densities were calculated by the rule of mixtures. The phase compositions and functional group analyses were identified by XRD and Fourier transform infrared spectroscopy (FTIR, UMA-600 Microscope, Varian, Palo Alto, CA, USA), respectively. To analyze the level of AMP dispersion within the PEEK matrix, cross-sections of the extruded filaments were viewed under SEM. Elemental analyses were carried out with energy dispersive X-ray spectroscopy (EDS, INCA, Oxford) at 20 kV and 15-mm working distance. Three samples per group were tested for the aforementioned analyses.

2.4. Thermal properties

Thermogravimetric (TG) and differential scanning calorimetry (DSC) curves of as-synthesized AMP were measured using a simultaneous thermal analyzer (SDT Q600, TA Instruments, Dallas, TA, USA) with a heating rate of 10°C/min. Melting temperatures and degree of crystallinity of the composites (n=3) were analyzed using DSC (PerkinElmer, Waltham, MA, USA). Approximately 5 mg of granulated PEEK or AMP-PEEK were

exposed to the following step-by-step program in a pure N_2 environment, namely Hold at 40°C for 3 min, Heat from 40°C to 370°C at 10°C/min, Hold at 370°C for 1 min, Cool from 370°C to 40°C at 100°C/min, Hold for 2 min at 40°C and Heat from 40°C to 370°C at 5°C/min. Data were acquired specifically from the final step.

The degree of crystallinity by weight (X_{CW}(%)) was evaluated using the equation:

$$Xcw(\%) = \frac{Hm}{Wf\ x\ Hc} \times 100$$

where, Hm is the melting enthalpy obtained from the DSC scan, Wf is the weight fraction of PEEK in the composite and ▲Hc is the melting enthalpy of fully crystallized PEEK (130 J.g $^{-1}$).

2.5. Rheological properties

Complex viscosity (η*), elastic modulus (G'), and viscous modulus (G") for PEEK and AMP-PEEK composites were determined using a rotational rheometer (ARES G2, TA Instruments, TA, USA). Oscillatory shear tests were conducted at 370°C, under N_2 environment, using 25 mm parallel plate geometry with a 1.2 mm gap spacing between the plates. To find the range where the elastic and viscous modulus are independent of the applied strain (i.e., the linear viscoelastic range, LVR), dynamic strain sweep tests were performed in the strain range of 0.1–100% at a constant frequency of 10 rad/s (figure S1). For dynamic frequency sweep measurements, 10% strain amplitude (such that it was within the limits of linear viscoelasticity and the optimum torque range of the transducer) and 0.1–500 rad/sec frequency range was selected.

2.6. Evaluation of *in vitro* bioactivity (Simulated body fluid, SBF)

We used a modified version (t-SBF) of the original Kokubo's composition (c-SBF) [18]. Bare PEEK (control) or AMP-PEEK specimens (n=3/group) were placed in containers filled with 15 ml of t-SBF and kept in a thermostatic water bath at 37°C for 7 days. The solution (t-SBF) was replenished every 24 h. Finally, after 7 days, the samples were retrieved, washed and dried at room temperature prior to further analyses. SEM, EDS and XRD (using the same operational parameters as described in Section 2.3.) were used to study the apatite-forming ability of the AMP-PEEK composites.

2.7. *In vitro* cytocompatibility studies

Mouse pre-osteoblasts (MC3T3-E1, CRL-2593™, ATCC, Manassas, VA, USA) were cultured in minimum essential medium (MEM-α, Thermo Scientific), supplemented with 10% fetal bovine serum (FBS, HyClone) and 1% penicillin/streptomycin (0.2 g/ml) at 5% CO_2 and 37°C. Triplicate samples were used per group, for each time point, were analyzed for all *in vitro* cell-related analyses.

2.7.1. Cell viability and proliferation—Thiazolyl blue tetrazolium bromide (MTT, Sigma Aldrich, St. Louis, MI, USA) was used to determine cytocompatibility. Sterile specimens (filaments of length 5 mm and diameter 2 mm), cells (2.3×10^4 cells/well) were

seeded on PEEK (control) or AMP-PEEK and cultured for 4, 7, or 14 days. At specified time periods, 500 μl MTT stock solution (12 mM) was added to the culture, followed by 4 h incubation at 5% CO_2 and 37°C. Dimethyl sulfoxide (DMSO) was used to dissolve formazan and OD_{570} readings were recorded using spectrophotometer (BioTek Instruments Inc., Winooski, VT, USA).

2.7.2. Osteogenic gene expression (qRT-PCR)—In this assay, MC3T3-E1 cells were seeded at 90% confluency in T75 flasks and further cultured on PEEK or AMP-PEEK specimens for 4 or 7 days. TRIzol reagent (Invitrogen) was used to extract the RNA from these cells and complementary DNA was produced by reverse transcription using M-MLV reverse transcriptase (Promega). qRT PCR was performed using SsoFast EvaGreen Supermix (Bio-Rad) by a 2-step amplification program (30 s at 95°C and 60 s at 62°C) on a thermal cycler (Eppendorf). The $2^{-\Delta\Delta CT}$ method was used to perform the relative quantification of mRNA of the genes and presented as fold-change compared to control samples. Glyceraldehyde 3-phosphate dehydrogenase (GAPDH) was used as the housekeeping gene.

2.7.3. Pre-osteoblast cell-material interaction—PEEK or AMP-PEEK specimens (filaments of 5-mm length and 2-mm diameter) were seeded with 6.5×10^4 cells/well. After a 4- or 7-day culture, the specimens were retrieved, washed in PBS and immersed in 3% glutaraldehyde solution for 1h at room temperature. Then, the specimens were incubated in ascending ethanol solutions (30–100%) followed by soaking in hexamethyldisilizane (HMDS). Subsequently, the specimens were left to dry overnight in a fume hood and sputter-coated with Au for SEM imaging [37].

2.8. *In vivo* implantation studies

2.8.1. Animal model of osseointegration—For *in vivo* analyses, PEEK or AMP-PEEK filaments (10-mm in length and 2-mm in diameter) were used. Bare PEEK was used as the control and 15AMP-PEEK (hereafter referred as AMP-PEEK) was chosen based on its *in vitro* cell-related results. Animal experiments were approved by the University of Michigan Institutional Animal Care and Use Committee (IACUC, protocol #PRO00008502). Twenty-four adult male rats (Fischer F344), 16-week-old (300–320 g) were obtained from Envigo RMS, Inc. (Oxford, MI, USA). Animals were kept in cages in groups of three, housed at 21°C ambient temperature and maintained in a light/dark cycle of 12/12h. Previous to the surgical procedures, general anesthesia induced with inhalation isoflurane (Piramal, Pennsylvania, USA) (4–5%) was performed. During the surgical procedures, the anesthesia was maintained with isoflurane (1–3%) using a calibrated vaporizer. The femur regions were shaved and scrubbed with chlorhexidine (2%). Incisions (2-cm) were made in the medial parapatellar regions with displacement and remoteness of the muscle complex. Drill diameters ranging from 2.0 – 2.5 mm were sequentially used under constant irrigation with sterile saline to perform the proximal epiphysis and to access the intramedullary canal. Autoclaved PEEK or AMP-PEEK composite specimens were press-fitted in the femur along the longitudinal axis through a medial parapatellar arthrotomy, filling the entire medullary canal (n=4/group/time point). Right femurs received PEEK implants and left femurs received AMP-PEEK implants. Post-surgery, animals were

medicated with non-steroidal anti-inflammatory drug (5 mg kg^{-1} Carprofen® base, Pfizer) subcutaneously. After 4 or 12 weeks, animals were euthanized, and the femurs were collected.

2.8.2. Micro-computed tomography (μ-CT)—After euthanasia, muscle tissue and epiphyses were removed. Bone/implants were fixed with 4% paraformaldehyde and non-destructive analysis of the newly formed bone at the implant interface was performed (Scanco μCT 100 Medical AG, Brüttisellen, Zurich, Switzerland). Samples were scanned with pieces rotation in 360°, using 70 kV, 114μA monochromatic X-rays and 25 μm voxel size. The exposure time was maintained to be 500 ms and 3 frames averaging was recorded. The Scanco Medical System software was used for image reconstruction. A region of interest (ROI) around the implants was defined. This was used to calculate “bone volume” (BV) and “bone implant contact” (BIC).

2.8.3. Histology—For histological analysis, non-demineralized samples were prepared. Bone-implant blocks were fixed in 10% formaldehyde followed by gradual dehydration using a series of ethanol solutions (70–100%). Specimens were processed using a tissue processor (Leica ASP300, Buffalo Grove, IL, USA) and subsequently placed into a series of methylmethacrylate and dibutylphthalate with progressively higher concentrations of benzoyl peroxide. Samples were manually embedded in partially polymerized methylmethacrylate (PMMA) and allowed to cure at room temperature. Blocks were then hardened at 37°C overnight. Tissues were sliced (~ 300 μm in thickness) through the center of the implant, glued to acrylic slides and allowed to set for 24 h prior to polishing procedures. Sections were then reduced to a final thickness of ~ 30 μm by grinding/polishing under water irrigation. Subsequently, sections were stained with toluidine blue and analyzed under an optical microscope. Images were captured at 20× magnification, and digital image analysis software (Image J v.1.45; National Institutes of Health, Bethesda, MD, USA) was used to measure the bone-to-implant contact (BIC) (overview at 2× and 4× with high magnification at 20× and 40×) (Olympus BX51, Melville, NY, USA).

2.8.4. Histomorphometric and BSE-SEM bone-implant contact analyses—Eight non-superimposing fields, corresponding to the bone/implant interface (four fields on each side of the implant), were captured by photographing each histological section at 20× magnification. The Image J software was used to measure bone-implant contact (BIC). In detail, bone-implant contact was calculated by subtracting BIC regions along the implant perimeter from the total implant perimeter. Results are reported as mean percentages and standard deviation. Immediately after histomorphometry analysis, the implant/bone interfaces were also examined by SEM (BSE-SEM, MIRA3, Tescan, Brno, Czechia) [38]. EDS was also performed (MIRA3, Tescan, Brno, Czechia).

2.9. Statistical analysis

For physical, chemical, and *in vitro* analyses, wherever applicable, results were represented as mean of 3 specimens ± standard deviation. One-way analysis of variance (ANOVA) with Tukey’s test was conducted using the Minitab software to determine the statistical difference between groups and $p<0.05$ were considered significant. For *in vivo* analyses, rat was the

unit analysis. Data obtained from *in vivo* experiments were evaluated by two-way ANOVA and post-hoc Tukey's test. Differences were considered statistically significant when $p<0.05$. The program GraphPad Prism version 8.0 was used for the analyses.

3. Results

3.1. AMP physical and thermal properties

Figures 2((a), (b) and (c)) present the phase, morphology, elemental and thermal analyses of AMP. As shown in figure 2(a), the wide and broad hump in the diffraction pattern of as-synthesized powders indicate the formation of an amorphous material. The amorphous nature of the bioceramic was retained up to 500°C. Heat treating at 600°C caused AMP to crystallize and form farringtonite ($Mg_3(PO_4)_2$, PDF: 98–001-4443). Additionally, the wide hump pertaining to the amorphous nature was present. Heat-treating AMP at 800°C resulted in the formation of single-phasic and highly crystalline farringtonite, as indicated by well-defined and sharp diffraction patterns. SEM image reveal irregular-shaped structures with edgeless boundaries (figure 2(b)). Further, the SEM micrograph (figure 2(b)) also denotes the presence of spherical particles either individually or coalesced with sheets. EDS analyses confirmed the presence of O, Mg and P with a 1.63 – 1.7 Mg/P atomic ratio. Figure 2(c) shows the TG and DSC results of as-synthesized AMP. The overall weight loss was gradual in nature and recorded to be 22%, most of it (20%) being from room temperature to 600°C. The primary weight loss can be associated with the removal of the absorbed water molecules in AMP during heating. DSC showed an exothermic peak at 702°C indicating crystallization of farringtonite.

3.2. Physical properties

The density measurements of various AMP-PEEK composites extruded at different processing temperatures are shown in figure 3(a). As expected, the addition of higher volume percentage of AMP (ρ = 1.5 g cm^{-3}) into PEEK (ρ =1.3 g cm^{-3}) resulted in the increase in density values of composites. However, the density values of specimens decreased with the increase in the extrusion temperatures. Figure 3(b) confirmed the similar nature of theoretical and experimental density of the specimens. Figure 3(c) displays the XRD patterns of un-modified PEEK and various AMP-PEEK composites. Low temperature patterns are featureless due to the dominant presence of amorphous phases. The FTIR data in figure 3(d) displayed several peaks related to the functional groups of PEEK as opposed to no peaks relevant to AMP. SEM micrographs in figure 3(e) reveal the cross-sectional morphology of un-modified and 15AMP-PEEK composite. As opposed to bare and smooth surfaces of the un-modified polymer, the low magnification images of the composites showed homogeneous dispersion of white particles throughout the PEEK matrix. High magnification micrographs in figure 3(e) reveal the presence of few irregularly- and mainly spherical-shaped AMP particles embedded in PEEK and associated chemical composition (EDS data). Well dispersed AMP particles were also seen on the surfaces of the as-extruded filaments (15AMP-PEEK, Figure 2e) as it is essential for osseointegration *in vivo*.

3.3. Thermal properties

The DSC curves of the composites processed at various temperatures and AMP content are plotted in figure 4(a). The melting peaks (endothermic) can be noticed in the curves along with T_m ranging from 338.20 to 338.91°C as shown in (table 2). The differences in T_m was negligible, but it was evident that T_m and $H_m$decreased with increasing AMP content. On the contrary, crystallinity increased from 25.38 to 28.76% with the increase in AMP. The same effect (crystallinity increase) was recorded when extrusion temperature was increased (table 3).

3.4. Rheological properties

The rheological properties are presented in figure 4(b). Dynamic frequency sweep tests were conducted to explore network formation. As seen in the plots, below 1 rad/s, complex viscosity (η^*) of the specimens increased with an increasing AMP content. For instance, 15AMP-PEEK exhibited a complex viscosity double to that of 0AMP-PEEK at 0.1 rad/s. However, shear thinning was stronger with more AMP content at higher frequencies. At 100 rad/s, the complex viscosity of 15AMP-PEEK was 20% lesser than 0AMP-PEEK. Further, η^* as a function of angular frequency (ω) in the shear thinning regime was fit to a power law model: $\eta^*=k\,\omega^{n-1}$, where k is the flow consistency index and n is the flow behavior index (figure S2). As can be seen in table 2, the “n” values were observed to be smaller than 1 (ranging from 0.2–0.4) in case of all the specimens. This indicated the behavior of the specimens as shear thinning fluids. With the increase in AMP content, the “n” values decreased slightly, suggesting thinning effect. Similarly, the addition of AMP influenced the elastic moduli (G’) and viscous moduli (G”) more prominently at low frequencies. With the increase in AMP, G’ and G” increased below the crossover frequency. However, at higher frequencies, G’ and G” were nearly independent of AMP loading. According to the theory of linear viscoelasticity, for homogeneous polymer melts, linear viscoelasticity at low frequencies (terminal zone) reflects fully relaxed polymer chains ($G'\sim\omega^2$ and $G''\sim\omega$) [39, 40]. However, for filled polymer systems, G’ and G” deviate from this behavior [41]. For PEEK, the deviation started with lower or no second phase and becomes more pronounced with the increase in the AMP content. Moreover, with an increase in AMP content, crossover frequency (relaxation time) and modulus decreased (Table S1).

3.5. *In vitro* bioactivity

The bioactivity of the composites was analyzed using *in vitro* SBF immersion method (figure 5). Spherical particles approximately 2 μm in diameter with textured surface were deposited on all specimens. However, as opposed to the lesser number of spherical particles formed on un-modified PEEK, abundant globules were observed on AMP-PEEK composites. Few regions exposing the actual composite surfaces could be seen for 5AMP-PEEK specimens; however, for 10AMP-PEEK and 15AMP-PEEK, the specimens’ surfaces were covered and packed with globular-like structures. Higher magnification SEM micrographs of globules revealed their texture which can be described as a characteristic flake-like morphology. The EDS spectra recorded from globules indicated the presence of high amounts of Ca, P and C. The average Ca/P ratio calculated was about 1.9 and traces of elements such as Cl, Mg and Na were also detected. XRD analysis of un-modified PEEK

and 15AMP-PEEK composite helped to identify the new phase formed after SBF immersion. No additional peaks were detected in the case of PEEK. On the contrary, broadened peaks pertaining to apatite ($Ca_{10}(PO_4)_6(OH)_2$, PDF:97–001-6742) were observed approximately at 2 angle of 25° and 33° in case of the composite (15AMP-PEEK). Overall, SEM, EDS and XRD analyses validate the formation of a homogeneous bone-like apatite layer, which confirms the bioactivity enhancement of PEEK due to AMP incorporation.

3.6. *In vitro* cell-material interaction

Figure 6(a) shows cell proliferation data on various composites as measured by the MTT method. After 4 or 7 days, AMP-PEEK composites exhibited higher OD readings than un-modified PEEK, thus supporting the fact that the AMP addition resulted in better pre-osteoblast cell proliferation. Of note, 10AMP-PEEK and 15AMP-PEEK specimens showed statistically significant increase in cell proliferation at both time points. The mRNA expressions of five distinct genes are presented (figure 6(b)). After 4 days, the fold-change in mRNA expressions was not significant in case of AMP-PEEK with respect to un-modified PEEK. Only OPN expression was higher in 15AMP-PEEK with respect to 0AMP-PEEK. After 7 days, the fold-changes in Col1, OCN, OPN and Runx2 expressions were significantly higher in 15AMP-PEEK as compared to un-modified PEEK. 10AMP-PEEK also showed significant increase in OCN and OPN expressions compared to 5AMP-PEEK and pristine PEEK. SEM micrographs display cell adhesion and proliferation on the distinct compositions (figure 7). Pre-osteoblasts were seen to adhere on all the specimens, regardless of the chemical composition; although fewer cells were seen on pristine PEEK when compared to AMP-modified PEEK. Overall, cells displayed a flattened morphology and formed a healthy network on the composite surfaces by the cytoplasmic extension and filopodia attachment. Individual cell outlines were clearly visible after 4 days. After 7 days, significant cell proliferation was seen for the AMP-PEEK composites, depicted as thick cell-sheets which engulfed and wrapped around the whole composite surface. On the other hand, a considerably thinner cell layer was observed over un-modified PEEK.

3.7. *In vivo* studies

We choose 15AMP-PEEK (AMP-PEEK) for the *in vivo* analysis as it showed the best *in vitro* bioactivity and cell function characteristics. Figure 8(a) shows high-resolution images and quantitative data obtained from micro-CT of the regions around un-modified PEEK and AMP-PEEK after 4- and 12-weeks post-implantation. The 3D reconstruction showed the formation of thick and compact new bone around AMP-modified PEEK implants at both time points. In comparison, minimal new bone formation was seen for un-modified PEEK. Notably, after 12 weeks, a significant amount of newly formed bone was found in AMP-PEEK implants (figures 8(a),(b)).

Figure 9(a) presents the histological analysis of the implanted region for all groups. After 4 weeks of healing, high magnification images revealed an immature bone matrix interposed between the implant and pristine bone, with discontinuities gap at the bone-implant interface for un-modified PEEK implants. Meanwhile, newly formed bone was better observed in direct contact with the implant surface of AMP-PEEK. In fact, the purple regions at the interface highlight new bone formation directly fused onto the composites within 4 weeks

(figure 9(a)). After 12 weeks, bone volume adjacent to un-modified PEEK implants was significantly less. On the other hand, a significant amount of new compact trabecular bone was found adjacent to AMP-PEEK implants. Further, high-magnification images show the formation of mineralized bone (indicated by deep-red regions) at the bone-implant contact region. Nevertheless, bone formation around AMP-PEEK implants appeared to be somehow more mature compared to that around un-modified PEEK implants at 4 weeks. These qualitative results were corroborated by subsequent quantitative histomorphometry. After 4 and 12 weeks, the AMP-PEEK implants exhibited BIC value almost 2 times higher when compared to PEEK (figure 9(b)).

Figure 10(a) shows the assessment of the implant osseointegration via BSE-SEM. After 4 weeks, BSE-SEM micrographs clearly confirmed a good integration between neighboring bone and AMP-PEEK implants. Further, the presence of new mineralized bone tissue (marked by yellow arrows) around the implant was evident. Such observations could not be made in case of PEEK implants. After 12 weeks, the micrographs confirmed considerably greater amount of new bone around AMP-PEEK. Figure 10(b) presents the EDS, SEM and BSE-SEM analyses of different areas. The combined analyses confirmed the formation of new bone and the presence of mineralized tissue in contact with the AMP-PEEK implant surface.

4. Discussion

The main purpose of this work was to develop PEEK-based composites with enhanced osseointegration ability to serve as feedstock for 3D printing of orthopedic and dental implants. To that end, we explored the novel bioactive family of MgPs as the second phase in the polymer (PEEK) matrix. We specifically chose AMP due to three reasons, i.e., its amorphous nature and originally nano-spherical particle size would be easy to homogeneously disperse in the polymer matrix, it was thermally stable (retain its amorphous character) at the melt-blending temperatures required for developing PEEK-based composites, and previous efforts have shown excellent bioactive properties.

In the present study, Mg^{2+} and PO_4^{3-} ions reacted in a highly basic (pH=10.3) aqueous/ethanol solution to spontaneously precipitate AMP at 37°C. The aqueous precipitation of MgPs is strictly dependent on temperature, pH and ion concentrations [22]. The synthesis of stabilized AMP has been challenging as opposed to the development of ACP, due to the high affinity of Mg^{2+} ions to bond with water molecules and form crystalline materials [42]. For instance, when we attempted to develop tri-MgP hydrate, macro-sheets of cattite spontaneously precipitated at room temperature [18]. Zhou et al. [42] took advantage of the microwave's low energy barrier to develop AMP nanospheres. On the contrary, Ostrowski [43] et al. developed a highly saturated solution and precipitated AMP spontaneously. The aqueous precipitation method used here is similar to that of Ostrowski with higher ionic concentrations than those utilized by either Tamimi [22] or Zhou [42]. The precipitates that form immediately remains amorphous while in solution but a rapid rinsing and drying is necessary to stabilize its amorphous state. Once dried, AMP can be stable under ambient conditions but thermal treatment above 500°C facilitated that energy required for the

materials to crystallize and form crystalline MgP confirmed by XRD (figure 2(a)). The DSC results (figure 2(c)) also confirmed that with the indication of an exothermic reaction peak.

Worth mentioning, the rationale for the thermal treatment studies presented herein was to ensure the thermal stability of AMP at the melt-blending temperatures of AMP-PEEK composites. In this study, 400°C was the highest processing temperature that could be used. As expected XRD did not detect any diffraction peaks corresponding to crystalline MgPs. This confirmed that the second phase retained their amorphous nature. FTIR did not reveal the functional groups of the bioceramic due to the low vol.% of AMP incorporation. However, the incorporation of the nano-spherical AMP particles within the PEEK matrix was confirmed by the SEM images (distributed white particles in figure 3(e)). AMP incorporation had a minor influence on the thermal properties of the composites. It is expected that during melt-blending, the processing temperature provides certain amount of thermal energy to the AMP particles to lose the absorbed water and initiate the phase transformation towards crystallization. This might have resulted in increasing the crystallinity of the composites containing AMP. Similarly, with the increase in processing temperature, the amount of transmitted thermal energy also increased, thus enhancing crystallinity of 10AMP-PEEK. However, the effect was not significant due to the low content of the second phase and the presence of PEEK matrix which acted as a thermal barrier for AMP. These results do not match with the studies involving HA-PEEK composites where crystallinity decreased with increasing temperatures [44]. The drop was attributed to the degradation of the polymeric chains in PEEK. On the contrary, the thermal analyses confirm that the AMP-PEEK composites did not show any signs of thermal degradation.

As previously stated, the present study aimed at developing an optimum AMP-PEEK composition to be used as feedstock for 3D printing. Due to the high melting point of PEEK, there are challenges in the arena of 3D printing. Hence, it is paramount to understand the rheology of the composites. At low frequencies, the enhancement in complex viscosity of the AMP-PEEK composites with an increase in AMP content can be attributed to the amplified second phase (AMP) network formations, polymer-particle and particle-particle interactions. Also, the onset of non-Newtonian behavior took place at lower frequencies. Similar phenomena have been observed in other composites [45–47]. Poslinski et al observed the increase in viscosity and the onset of shear thinning occurs at low frequencies, when micron-sized glass spheres were added to polymer network [48]. In the present case, at high frequencies, it is hypothesized that the network formed between the AMP nano-spheres were destroyed due to higher deformation rates, and also the randomly oriented polymer chains became aligned in the direction of the flow. At these conditions, the composites exhibited a decrease in viscosity (shear thinning) with η^* values very close to those of un-modified PEEK. Similar η^* trend had been reported in the literature for carbon nanotube filled and nano-clay filled PEEK composites with various second phase concentrations [41, 47, 49].

Within most of the frequency range, all AMP-PEEK composites exhibited viscoelastic behavior. Specifically, G” was larger than G’, and both moduli increased with the increase in frequency. Modulus crossover provides valuable information when converted to relaxation

times. The relaxation time (table S1) increased from 0.08 s to 0.26 s with increase in AMP. This might have resulted from elevated particle-particle and polymer-particle interactions at higher AMP content, which restricted polymer chain motions within the composite. The same interactions might be the reason for the deviation of composite properties from the linear viscoelasticity theory [47]. Further, all composites exhibited non-terminal behavior ($G' \sim \omega^{0.9-1.1}$ and $G'' \sim \omega^{0.65-0.75}$) with more deviation in scaling exponent at higher AMP contents, similar to previous results [41, 46, 47, 49–52].

From a printability standpoint, polymer viscosity plays an important role in material flowability through the printer nozzle. More importantly, the orientation of the final interface between the layers matters [53]. At low frequencies, higher AMP content caused an increase in specimen viscosity. High viscosity in the low-shear region is desirable for 3D printing applications to maintain the shape of the printed layers after deposition [54, 55]. At high frequency, however, composites with high AMP contents have more pronounced shear thinning and low viscosity. In 3D printing processes, good shear thinning behavior and low viscosity in the high-shear region are expected to both smoothen the material flow through the nozzle and improve the coalesce of the molten polymer into solid, uniform 3D printed structures [53, 54]. Therefore, rheology analyses of AMP-PEEK composites indicate a good fit with the required rheology for 3D printing of these materials. Very recently we were successful in developing cytocompatible and custom-designed PEEK-based orthopedic implants via 3D printing [34]. Notably, we intend to develop bioactive AMP-PEEK implants by 3D printing. Prior to that, it is first important to analyze the material, rheological and biological properties of the AMP-PEEK filaments by itself and determine the most suitable composition for 3D printing.

In case of orthopedic implants, bioactivity is one of the most important attributes. It dictates their ability to osseointegrate. The higher rate of apatite forming ability in SBF by AMP-PEEK as compared to PEEK predicts a faster *in vivo* bone binding capability of the AMP-PEEK implants [56]. Previous studies have shown the *in vitro* dissolution and re-precipitation of MgP phases in SBF [57] but no such observations were made in the present case. It was difficult to determine the dissolution of AMP embedded in the PEEK matrix as the surfaces were completely covered with a thick apatite-like layer within 7 days (figure 5). It is interesting to note that similar amount of apatite was formed on PEEK/nano-flurohydroxyapatite (FHA) composites only after 14 days [24], suggesting the enhanced bioactivity of AMP when compared to FHA [16].

In addition to the bioactivity tests, preliminary *in vitro* cell studies are important to determine the cytocompatibility of the composites prior to *in vivo* studies. Indeed, the presence of AMP in PEEK had a good effect on pre-osteoblast cell proliferation. Similar results were obtained by Zhou et al. [58] when MC3T3 pre-osteoblasts were cultured on PLA-AMP composites. Importantly, the results were comparable to PLA-HA composites. In other instances, AMP significantly promoted better cell proliferation compared to HA [23] and comparable cell viability to β-TCP [43]. This positive effect can be attributed to the presence of Mg^{2+} ions which are well-known for their favorable effect on cellular activities [18, 59, 60]. Furthermore, Mg^{2+} ions released during the dissolution of incorporated AMP were observed to influence osteogenic differentiation. Similar results were reported by

previous studies involving AMP [16, 23, 58]. The expression levels of all the markers studied herein increased with time and AMP content. The fold-changes were the highest for OPN followed by OCN, Col 1, Runx2 and ALP. Col 1 is a gene related to the formation of extracellular matrix and it is actively upregulated during proliferation but declines during mineralization. Both OPN and OCN are expressed after cellular proliferation. However, OPN is expressed in mineralization stage as well. Therefore, if AMP is expected to provide enhanced bioactivity, OPN should have the highest expression levels. Runx2 is a critical osteogenesis transcription factor. It is expressed and activated via activation of MAP kinase ERK1 and ERK2 and further activates ALP, OPN and OCN. While higher Runx2 expression levels explains results for OPN and OCN, the relatively lesser extent of ALP signifies lack of Ca^{2+} uptake from medium or inhibition effect of β-glycerophosphate induced ALP activity by high Mg^{2+} presence [58].

The *in vivo* behavior of the implanted biomaterials further attests the *in vitro* results and confirmed superior osseointegration capability of AMP-PEEK composites. It is worth mentioning that this is the first study to report the *in vivo* behavior of PEEK implants containing AMP. The significant amount of new bone formation as analyzed by micro-CT, might be attributed to the release of Mg^{2+} ions from AMP (figures 8(a), (b)) near the AMP-PEEK implant. At the end of 12 weeks, the increase of BV in case of AMP-PEEK composites was almost four times higher compared to PEEK. These results were corroborated by histomorphometry (figure 9(b)) confirming that AMP incorporation played a significant role in bone formation around the AMP-PEEK implant. Moreover, the histology results presented a qualitative analysis of the integration of the newly formed bone with the AMP-PEEK composites and greater amount of new bone formation when compared to PEEK. Importantly, after 12 weeks, AMP-PEEK showed the presence of compact and mature trabecular bone suggesting enhanced osseointegration. Toluidine blue staining reveals the proteoglycan content of tissues and is a useful tool for identifying regions of mature and immature bone due to their relative differences in organic content. Moreover, one can easily differentiate unmineralized osteoid from fully mineralized bone tissue and provides sufficient preservation of morphological details [61]. General observation showed that toluidine blue stained samples presented the same pattern (figure 9(a)). This pattern included more staining of regions close to the implant surface and less staining at regions away from the implant surface. It should also be noted that a sharp transition between newly formed bone and mature bone not affected by surgical trauma, was easily identified in all samples. Further, the presence of osteocytes indicated in light purple color (figure 9(a)) included in the bone matrix near the implant surface region indicated high bone maturity levels after 12 weeks. Further, the presence of a stable layer (as shown in figures 10(a), (b)) at the implant-bone interface in case of AMP-PEEK implants might have an important role in achieving superior osseointegration.

5. Conclusion

In this study, AMP-PEEK composite filaments were successfully developed via melt-blending technique. The AMP particles were homogeneously dispersed throughout the PEEK matrix and the AMP particles did not experience any thermal degradation during the high-temperature processing. The rheological studies confirmed that AMP-PEEK

composites are good candidates for 3D printing for exhibiting high zero-shear and low infinite-shear viscosities. Indeed, the incorporation of AMP enhanced PEEK's bioactivity and helped in significant increase of pre-osteoblast adhesion and proliferation. The presence of Mg^{2+} ions magnified important gene expression markers like Col1, OCN and OPN. Further, when implanted *in vivo*, AMP-PEEK implants exhibited enhanced osseointegration with significant increased new bone formation surrounding the implants as opposed to PEEK. Collectively, the present investigation demonstrated that AMP-PEEK composite filaments can serve as feedstock for 3D printing of orthopedic and dental implants due to enhanced bioactivity and osseointegration.

Supplementary Material

Refer to Web version on PubMed Central for supplementary material.

Acknowledgements

The authors deny any conflicts of interest related to this study. S.B.B. and P.S. acknowledges the National Science Foundation (NSF grant #1706513). S.B.B. is also supported by an NSF IR/D grant mechanism. M.C.B. acknowledges the National Institutes of Health (NIH, National Institute of Dental and Craniofacial Research/NIDCR, grants K08DE023552 and R01DE026578). S.B.B. and M.C.B. would like to thank the support of Academy of Osseointegration - Osseointegration Foundation Research Grant, International Association for Dental Research/Osseointegration Foundation – Implant Innovation Award. E.A.F. and M.W.L. acknowledge the U.S. Army Research Office (DURIP W911NF-15–1-0404). The content is solely the responsibility of the authors and does not necessarily represent the official views of the National Institutes of Health or National Science Foundation.

References

[1]. Jung HD, Jang TS, Lee JE, Park SJ, Son Y and Park SH 2019 Enhanced bioactivity of titanium-coated polyetheretherketone implants created by a high-temperature 3D printing process Biofabrication 11 045014

[2]. Kurtz SM and Devine JN 2007 PEEK biomaterials in trauma, orthopedic, and spinal implants Biomaterials 28 4845–69 [PubMed: 17686513]

[3]. Najeeb S, Zafar MS, Khurshid Z and Siddiqui F 2016 Applications of polyetheretherketone (PEEK) in oral implantology and prosthodontics Journal of prosthodontic research 60 12–9 [PubMed: 26520679]

[4]. Briem D, Strametz S, Schröder K, Meenen NM, Lehmann W, Linhart W, Ohl A and Rueger JM 2005 Response of primary fibroblasts and osteoblasts to plasma treated polyetheretherketone (PEEK) surfaces J Mater Sci Mater Med 16 671–7 [PubMed: 15965600]

[5]. Noiset O, Schneider YJ and Marchand-Brynaert J 1999 Fibronectin adsorption or/and covalent grafting on chemically modified PEEK film surfaces J Biomater Sci Polym Ed 10 657–77 [PubMed: 10385226]

[6]. Mishra S and Chowdhary R 2019 PEEK materials as an alternative to titanium in dental implants: A systematic review Clinical implant dentistry and related research 21 208–22 [PubMed: 30589497]

[7]. Schwitalla A and Müller W-D 2013 PEEK dental implants: a review of the literature Journal of Oral Implantology 39 743–9 [PubMed: 21905892]

[8]. Ma R and Tang T 2014 Current strategies to improve the bioactivity of PEEK International journal of molecular sciences 15 5426–45 [PubMed: 24686515]

[9]. Najeeb S, Khurshid Z, Matinlinna JP, Siddiqui F, Nassani MZ and Baroudi K 2015 Nanomodified peek dental implants: Bioactive composites and surface modification—A review International journal of dentistry 2015

[10]. Abdullah MR, Goharian A, Abdul Kadir MR and Wahit MU 2015 Biomechanical and bioactivity concepts of polyetheretherketone composites for use in orthopedic implants—a review Journal of Biomedical Materials Research Part A 103 3689–702 [PubMed: 25856801]

[11]. Hotchkiss KM, Reddy GB, Hyzy SL, Schwartz Z, Boyan BD and Olivares-Navarrete R 2016 Titanium surface characteristics, including topography and wettability, alter macrophage activation Acta Biomater 31 425–34 [PubMed: 26675126]

[12]. Surmenev RA, Surmeneva MA and Ivanova AA 2014 Significance of calcium phosphate coatings for the enhancement of new bone osteogenesis–a review Acta biomaterialia 10 557–79 [PubMed: 24211734]

[13]. Nabiyouni M, Brückner T, Zhou H, Gbureck U and Bhaduri SB 2018 Magnesium-based bioceramics in orthopedic applications Acta biomaterialia 66 23–43 [PubMed: 29197578]

[14]. Zhou H, Goel VK and Bhaduri SB 2014 A fast route to modify biopolymer surface: a study on polyetheretherketone (PEEK) Materials Letters 125 96–8

[15]. Koju N, Sikder P, Ren Y, Zhou H and Bhaduri SB 2017 Biomimetic coating technology for orthopedic implants Current opinion in chemical engineering 15 49–55

[16]. Ren Y, Sikder P, Lin B and Bhaduri S B 2018 Microwave assisted coating of bioactive amorphous magnesium phosphate (AMP) on polyetheretherketone (PEEK) Materials Science and Engineering: C 85 107–13 [PubMed: 29407138]

[17]. Bhaduri S B, Goel VK, Ren Y and Sikder P 2018 Bifunctional Bioactive Antibacterial Coatings, and Process for Coating Implant Surfaces Therewith. Google Patents)

[18]. Sikder P, Grice CR, Lin B, Goel VK and Bhaduri SB 2018 Single-Phase, Antibacterial Trimagnesium Phosphate Hydrate Coatings on Polyetheretherketone (PEEK) Implants by Rapid Microwave Irradiation Technique ACS Biomaterials Science & Engineering 4 2767–83

[19]. Sader MS, LeGeros RZ and Soares GA 2009 Human osteoblasts adhesion and proliferation on magnesium-substituted tricalcium phosphate dense tablets Journal of Materials Science: Materials in Medicine 20 521–7 [PubMed: 18987959]

[20]. Zhao S f, Jiang Q h, Peel S, Wang X x and He F m 2013 Effects of magnesium-substituted nanohydroxyapatite coating on implant osseointegration Clinical oral implants research 24 34–41 [PubMed: 22145854]

[21]. Combes C and Rey C 2010 Amorphous calcium phosphates: synthesis, properties and uses in biomaterials Acta biomaterialia 6 3362–78 [PubMed: 20167295]

[22]. Tamimi F, Le Nihouannen D, Bassett DC, Ibasco S, Gbureck U, Knowles J, Wright A, Flynn A, Komarova SV and Barralet JE 2011 Biocompatibility of magnesium phosphate minerals and their stability under physiological conditions Acta biomaterialia 7 2678–85 [PubMed: 21324383]

[23]. Nabiyouni M, Ren Y and Bhaduri SB 2015 Magnesium substitution in the structure of orthopedic nanoparticles: A comparison between amorphous magnesium phosphates, calcium magnesium phosphates, and hydroxyapatites Materials Science and Engineering: C 52 11–7 [PubMed: 25953534]

[24]. Wang L, He S, Wu X, Liang S, Mu Z, Wei J, Deng F, Deng Y and Wei S 2014 Polyetheretherketone/nano-fluorohydroxyapatite composite with antimicrobial activity and osseointegration properties Biomaterials 35 6758–75 [PubMed: 24835045]

[25]. Monich PR, Henriques B, de Oliveira APN, Souza JC and Fredel MC 2016 Mechanical and biological behavior of biomedical PEEK matrix composites: A focused review Materials Letters 185 593–7

[26]. Wong K, Wong C, Liu W, Pan H, Fong M, Lam W, Cheung W, Tang W, Chiu K and Luk K 2009 Mechanical properties and in vitro response of strontium-containing hydroxyapatite/polyetheretherketone composites Biomaterials 30 3810–7 [PubMed: 19427032]

[27]. Ma R, Tang S, Tan H, Lin W, Wang Y, Wei J, Zhao L and Tang T 2014 Preparation, characterization, and in vitro osteoblast functions of a nano-hydroxyapatite/polyetheretherketone biocomposite as orthopedic implant material International journal of nanomedicine 9 3949 [PubMed: 25170265]

[28]. Bakar M A, Cheng M, Tang S, Yu S, Liao K, Tan C, Khor K and Cheang P 2003 Tensile properties, tension–tension fatigue and biological response of polyetheretherketone–

hydroxyapatite composites for load-bearing orthopedic implants Biomaterials 24 2245–50 [PubMed: 12699660]

[29]. Ma R, Weng L, Bao X, Song S and Zhang Y 2013 In vivo biocompatibility and bioactivity of in situ synthesized hydroxyapatite/polyetheretherketone composite materials Journal of Applied Polymer Science 127 2581–7

[30]. Tan K, Chua C, Leong K, Cheah C, Cheang P, Bakar M A and Cha S 2003 Scaffold development using selective laser sintering of polyetheretherketone–hydroxyapatite biocomposite blends Biomaterials 24 3115–23 [PubMed: 12895584]

[31]. Wang L, Weng L, Song S and Sun Q 2010 Mechanical properties and microstructure of polyetheretherketone–hydroxyapatite nanocomposite materials Materials Letters 64 2201–4

[32]. Converse GL, Conrad TL, Merrill CH and Roeder RK 2010 Hydroxyapatite whisker-reinforced polyetherketoneketone bone ingrowth scaffolds Acta biomaterialia 6 856–63 [PubMed: 19665061]

[33]. Petrovic L, Pohle D, Münstedt H, Rechtenwald T, Schlegel K and Rupprecht S 2006 Effect of βTCP filled polyetheretherketone on osteoblast cell proliferation in vitro Journal of biomedical science 13 41–6 [PubMed: 16228286]

[34]. Elhattab K, Sikder P, Walker J, Bottino M and Bhaduri S 2019 Fabrication and Evaluation of 3-D Printed PEEK Scaffolds Containing Macropores by Design Materials Letters 127227

[35]. Rodrigues A and Lebugle A 1998 Influence of ethanol in the precipitation medium on the composition, structure and reactivity of tricalcium phosphate Colloids and Surfaces A: Physicochemical and Engineering Aspects 145 191–204

[36]. Babaie E, Zhou H, Lin B and Bhaduri SB 2015 Influence of ethanol content in the precipitation medium on the composition, structure and reactivity of magnesium–calcium phosphate Materials Science and Engineering: C 53 204–11 [PubMed: 26042708]

[37]. Sikder P, Koju N, Ren Y, Goel VK, Phares T, Lin B and Bhaduri SB 2018 Development of single-phase silver-doped antibacterial CDHA coatings on Ti6Al4V with sustained release Surface and Coatings Technology 342 105–16

[38]. Bottino MC, Coelho PG, Henriques VA, Higa OZ, Bressiani AH and Bressiani J C 2009 Processing, characterization, and in vitro/in vivo evaluations of powder metallurgy processed Ti-13Nb-13Zr alloys Journal of Biomedical Materials Research Part A: An Official Journal of The Society for Biomaterials, The Japanese Society for Biomaterials, and The Australian Society for Biomaterials and the Korean Society for Biomaterials 88 689–96

[39]. Ottenbrite RM, Utracki LA and Inoue S 1987 Current Topics in Polymer Science: Polymer chemistry and polymer physics vol 1: Munich: Hanser Publishers; Don Mills, Ont.: Distributed in Canada by Collier …)

[40]. Senanayake KK, Fakhrabadi EA, Liberatore MW and Mukhopadhyay A 2019 Diffusion of Nanoparticles in Entangled Poly(vinyl alcohol) Solutions and Gels Macromolecules

[41]. Bangarusampath DS, Ruckdaschel H, Altstadt V, Sandler JKW, Garray D and Shaffer MSP 2009 Rheology and properties of melt-processed poly(ether ether ketone)/multi-wall carbon nanotube composites Polymer 50 5803–11

[42]. Zhou H, Luchini TJ and Bhaduri SB 2012 Microwave assisted synthesis of amorphous magnesium phosphate nanospheres Journal of Materials Science: Materials in Medicine 23 2831–7 [PubMed: 22890518]

[43]. Ostrowski N, Lee B, Hong D, Enick PN, Roy A and Kumta PN 2014 Synthesis, osteoblast, and osteoclast viability of amorphous and crystalline tri-magnesium phosphate ACS Biomaterials Science & Engineering 1 52–63

[44]. Bakar MA, Cheang P and Khor K 1999 Thermal processing of hydroxyapatite reinforced polyetheretherketone composites Journal of Materials Processing Technology 89 462–6

[45]. Frigione M, Naddeo C and Acierno D 1997 The rheological behavior of polyetheretherketone (PEEK) polyetherimide (PEI) blends J Polym Eng 16 217–29

[46]. Su Y, Wang T, Dang G, Zhou H and Chen C 2016 The effects of manganese ions on rheology and thermal properties of polyether ether ketone High Performance Polymers 29 377–85

[47]. Agarise C 2009 Rheological Characterization and Modeling of Micro- and Nano-Scale Particle Suspensions. (OhioLINK Electronic Theses and Dissertations Center: Ohio State University)

[48]. Poslinski AJ, Ryan ME, Gupta RK, Seshadri SG and Frechette FJ 1988 Rheological Behavior of Filled Polymeric Systems I. Yield Stress and Shear-Thinning Effects Journal of Rheology 32 703–35

[49]. Bangarusampath DS, Ruckdaschel H, Altstadt V, Sandler JKW, Garray D and Shaffer MSP 2009 Rheological and electrical percolation in melt-processed poly(ether ether ketone)/multi-wall carbon nanotube composites Chemical Physics Letters 482 105–9

[50]. Bokobza L 2007 Multiwall carbon nanotube elastomeric composites: A review Polymer 48 4907–20

[51]. Indu Shekar R, Satheesh Kumar MN, Damodhara Rao PM, Yaakob Z, Kotresh TM, Siddaramaiah and Chandrakala 2011 Studies on the composites produced from co-weaved poly ether ether ketone and glass fiber fabric Journal of Composite Materials 45 741–9

[52]. Yuan MJ, Galloway JA, Hoffman RJ and Bhatt S 2011 Influence of Molecular Weight on Rheological, Thermal, and Mechanical Properties of PEEK Polymer Engineering and Science 51 94–102

[53]. Blok LG, Longana ML, Yu H and Woods BKS 2018 An investigation into 3D printing of fibre reinforced thermoplastic composites Additive Manufacturing 22 176–86

[54]. Nguyen NA, Bowland CC and Naskar AK 2018 A general method to improve 3D-printability and inter-layer adhesion in lignin-based composites Applied Materials Today 12 138–52

[55]. Stepashkin AA, Chukov DI, Senatov FS, Salimon AI, Korsunsky AM and Kaloshkin SD 2018 3D-printed PEEK-carbon fiber (CF) composites: Structure and thermal properties Composites Science and Technology 164 319–26

[56]. Kokubo T and Takadama H 2006 How useful is SBF in predicting in vivo bone bioactivity? Biomaterials 27 2907–15 [PubMed: 16448693]

[57]. Ren Y, Babaie E, Lin B and Bhaduri SB 2017 Microwave-assisted magnesium phosphate coating on the AZ31 magnesium alloy Biomedical Materials 12 045026

[58]. Zhou H, Nabiyouni M, Lin B and Bhaduri SB 2013 Fabrication of novel poly (lactic acid)/ amorphous magnesium phosphate bionanocomposite fibers for tissue engineering applications via electrospinning Materials Science and Engineering: C 33 2302–10 [PubMed: 23498262]

[59]. Sikder P, Grice C and Bhaduri SB 2019 Processing-structure-property correlations of crystalline antibacterial magnesium phosphate (newberyite) coatings and their in vitro effect Surface and Coatings Technology

[60]. Sikder P, Bhaduri SB, Ong JL and Guda T 2019 Silver (Ag) doped magnesium phosphate microplatelets as next-generation antibacterial orthopedic biomaterials Journal of Biomedical Materials Research Part B: Applied Biomaterials

[61]. Grizon F, Aguado E, Hure G, Baslé M and Chappard D 2002 Enhanced bone integration of implants with increased surface roughness: a long term study in the sheep Journal of dentistry 30 195–203 [PubMed: 12450710]

Highlights

- The composite filaments were successfully developed via melt-blending technique.
- AMP-PEEK filaments can serve as feedstock for 3D printing of patient-specific implants.
- The bioactivity of the composites significantly increased cell adhesion and proliferation.
- AMP-PEEK facilitate *in vivo* osseointegration and suitable bone regeneration capabilities.

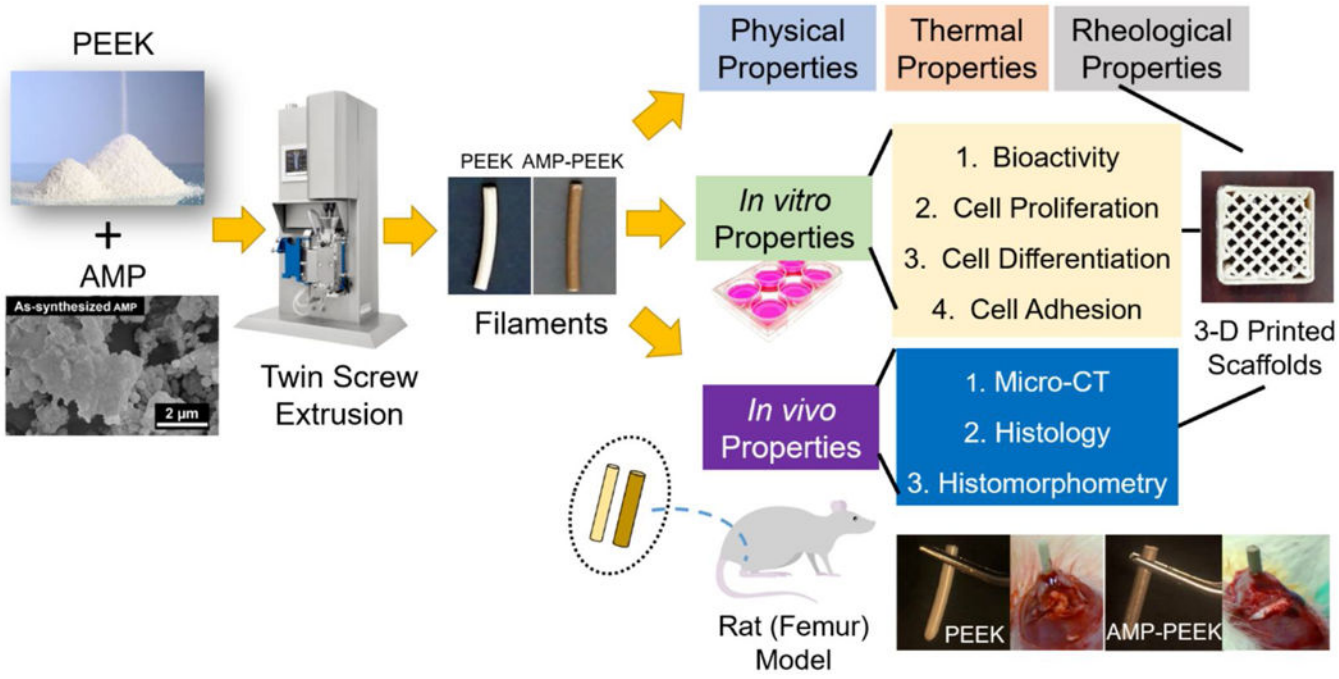

Figure 1.

Schematic illustration of the fabrication steps as well as physical, thermal, rheological and biological characterizations of AMP-PEEK composite filaments for 3D printing applications.

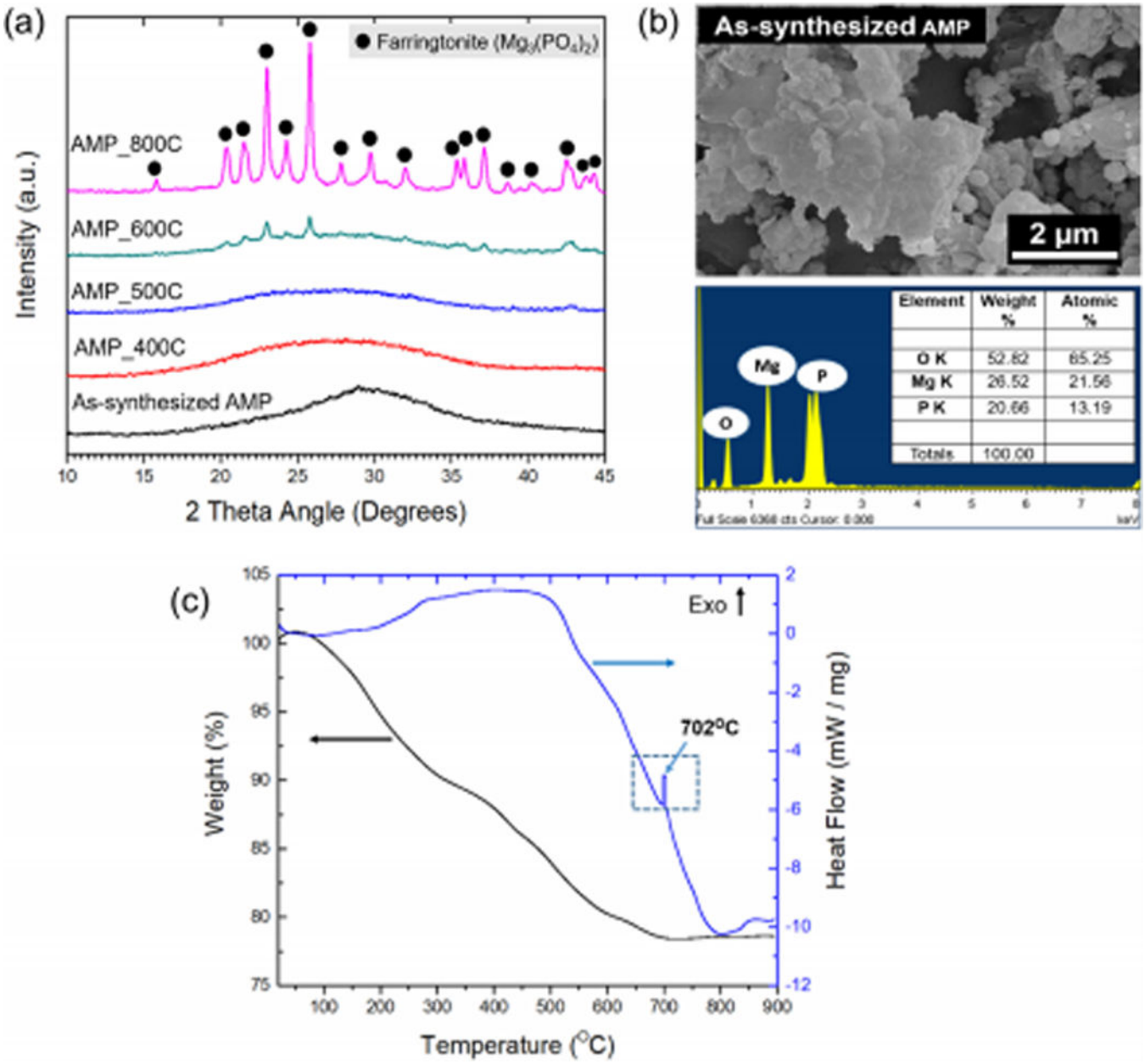

Figure 2.

Different properties of amorphous magnesium phosphate (AMP). **(a)** X-ray diffraction (XRD) analysis and **(b)** Scanning electron microscopy (SEM) of as-synthesized AMP. **(c)** Thermogravimetric (TG) and heat flow curve of AMP.

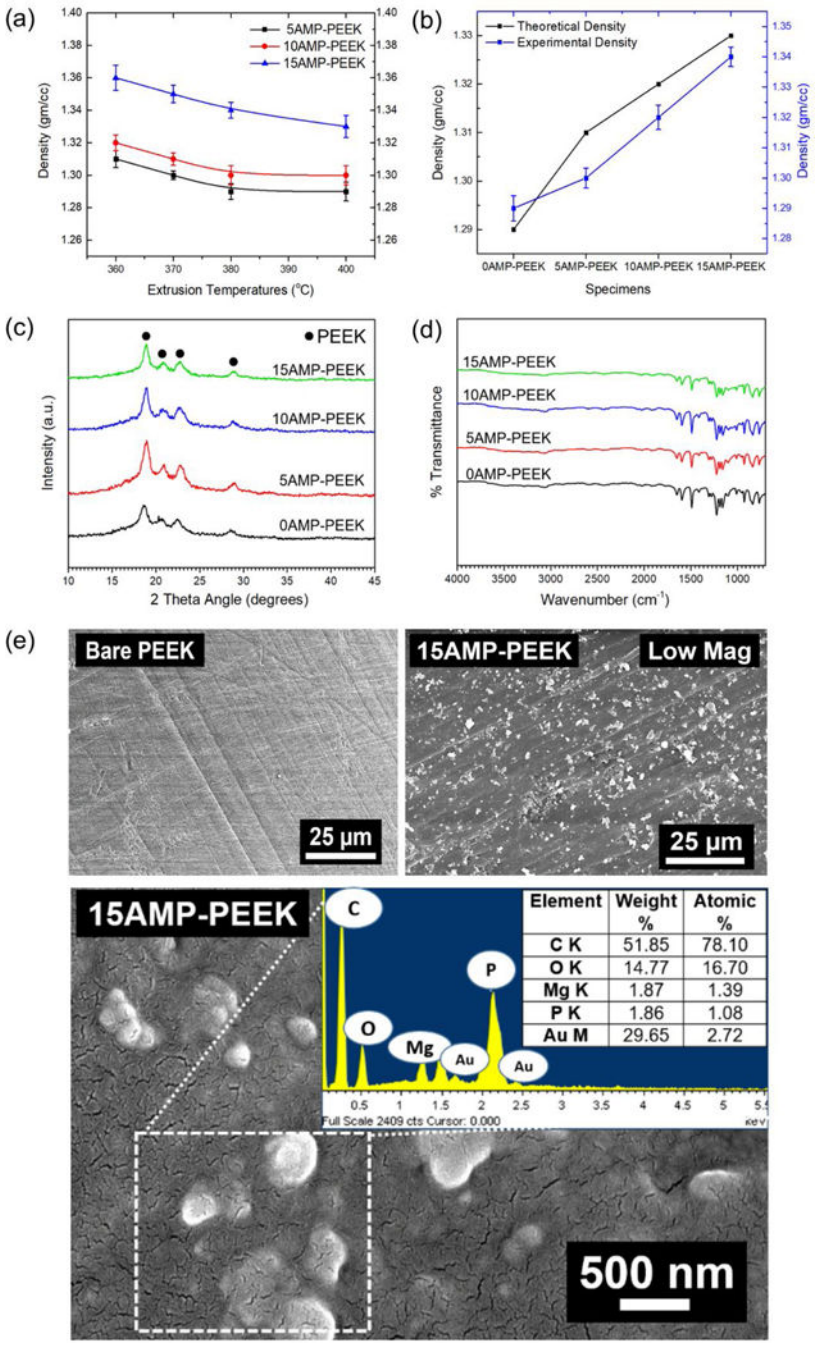

Figure 3.

Physical properties of AMP-PEEK composites. **(a)** Density of various AMP-PEEK composites processed at different melt-blending temperatures. **(b)** Theoretical and experimental density of AMP-PEEK composites processed at 370 °C. **(c)** XRD, **(d)** FTIR and **(e)** SEM analysis of bare PEEK and 15AMP-PEEK composites. The inset in the SEM micrograph contains the EDS analysis of the dotted box. Of note, the white particles indicating AMP are homogenously dispersed in the PEEK matrix.

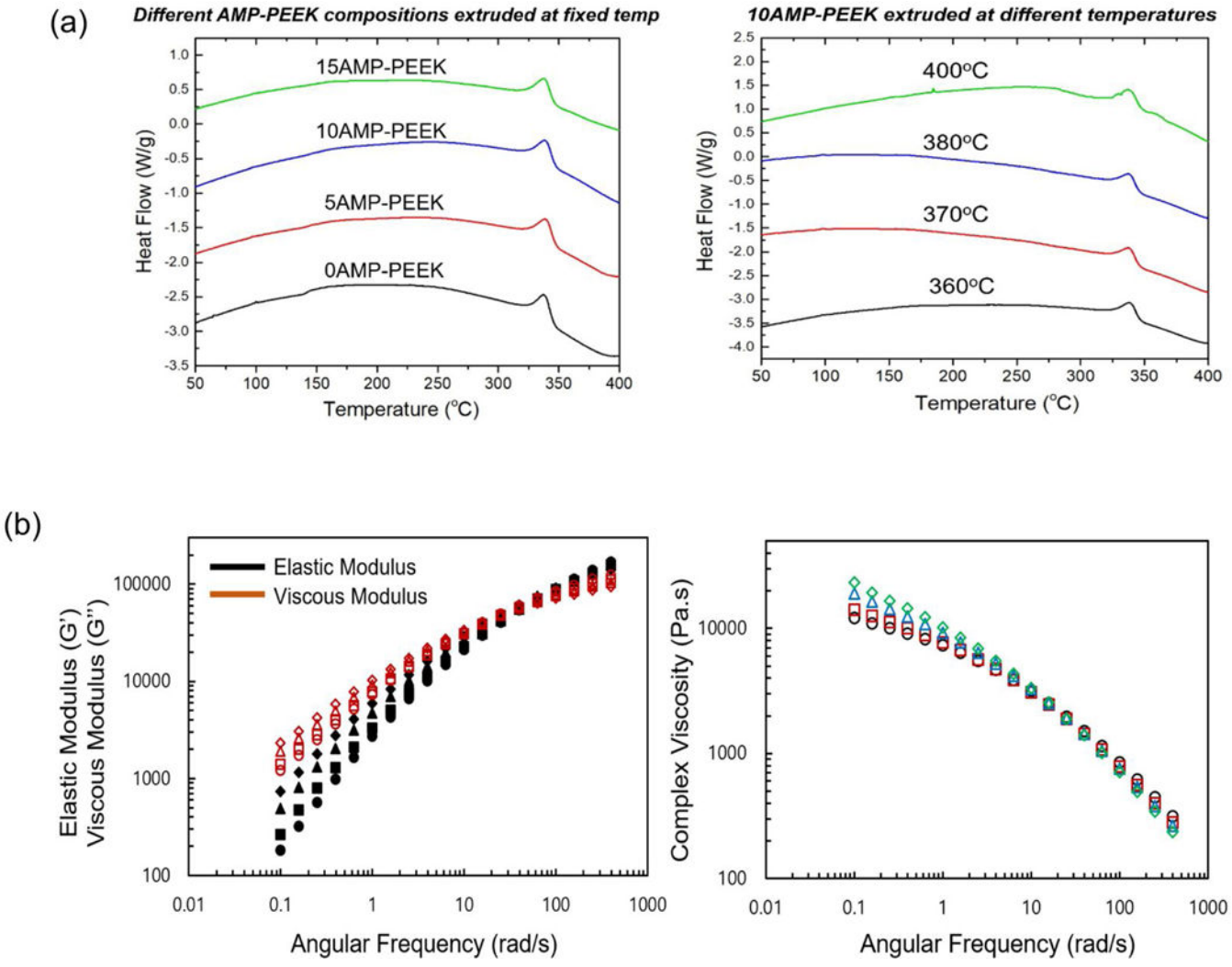

Figure 4.

a) Thermal properties of AMP-PEEK composites. Heat Flow curves of 10AMP-PEEK composites processed at different melt-blending temperatures and various composites with varying AMP content (adjacent). **(b)** Rheological properties of PEEK and AMP-PEEK specimens. Complex viscosity(η*), Elastic Modulus (G') and Viscous Modulus (G") are recorded. Symbols- For the left-side figure: Filled: Elastic Modulus, Empty: Viscous Modulus; For the right side figure: Diamond: 15AMP-PEEK, Triangle: 10AMP-PEEK, Square: 5AMP-PEEK, Circle: 0AMP-PEEK.

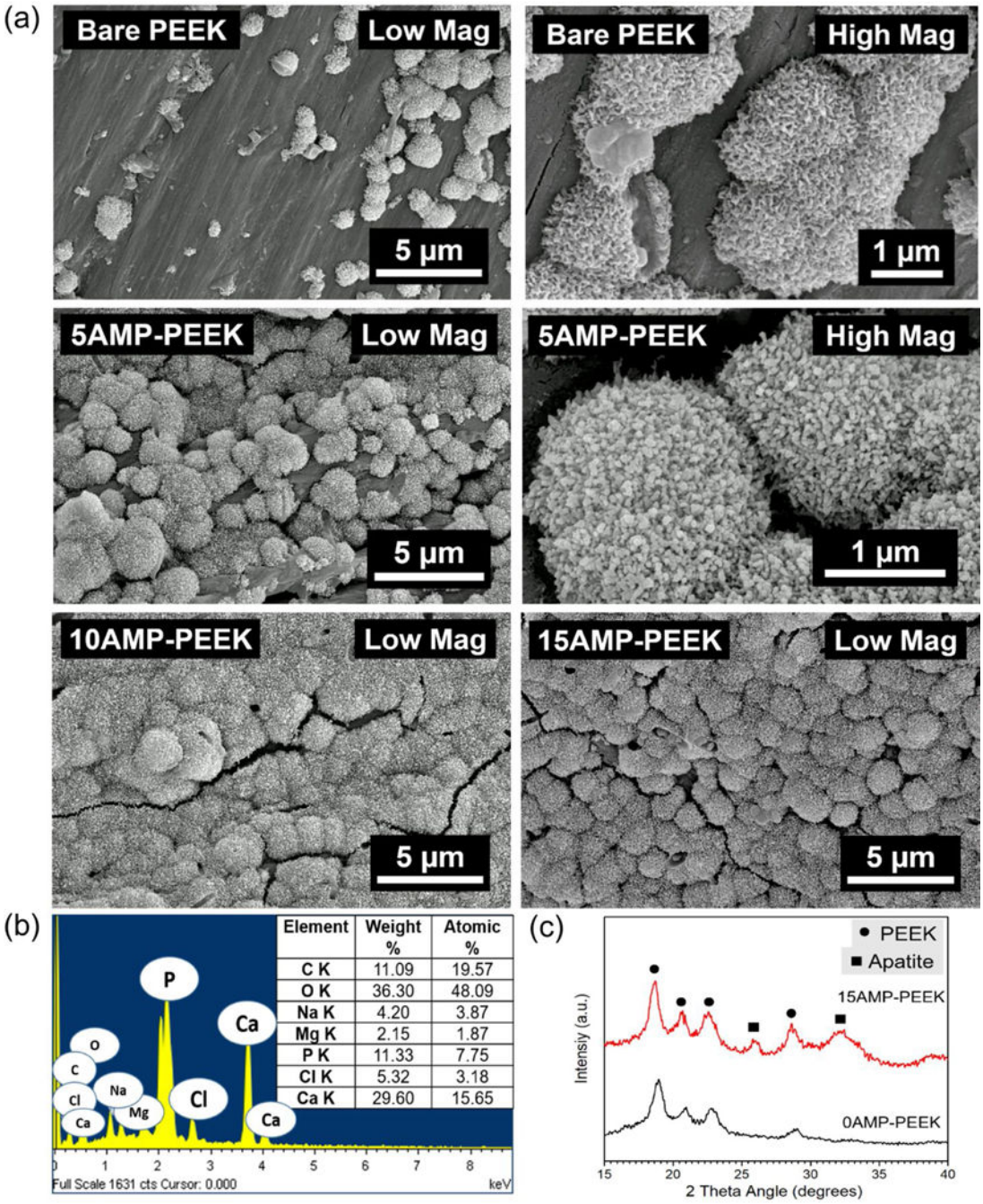

Figure 5.

Simulated Body Fluid (SBF) immersion results. SEM, EDS and XRD analysis of various AMP-PEEK composites after immersing in SBF for 7 days at 37 °C. Of note, is the formation of abundant globules with nano flake-like morphology as opposed to scanty presence of globules on bare PEEK. XRD also detects the formation of apatite peaks only on AMP-PEEK specimen.

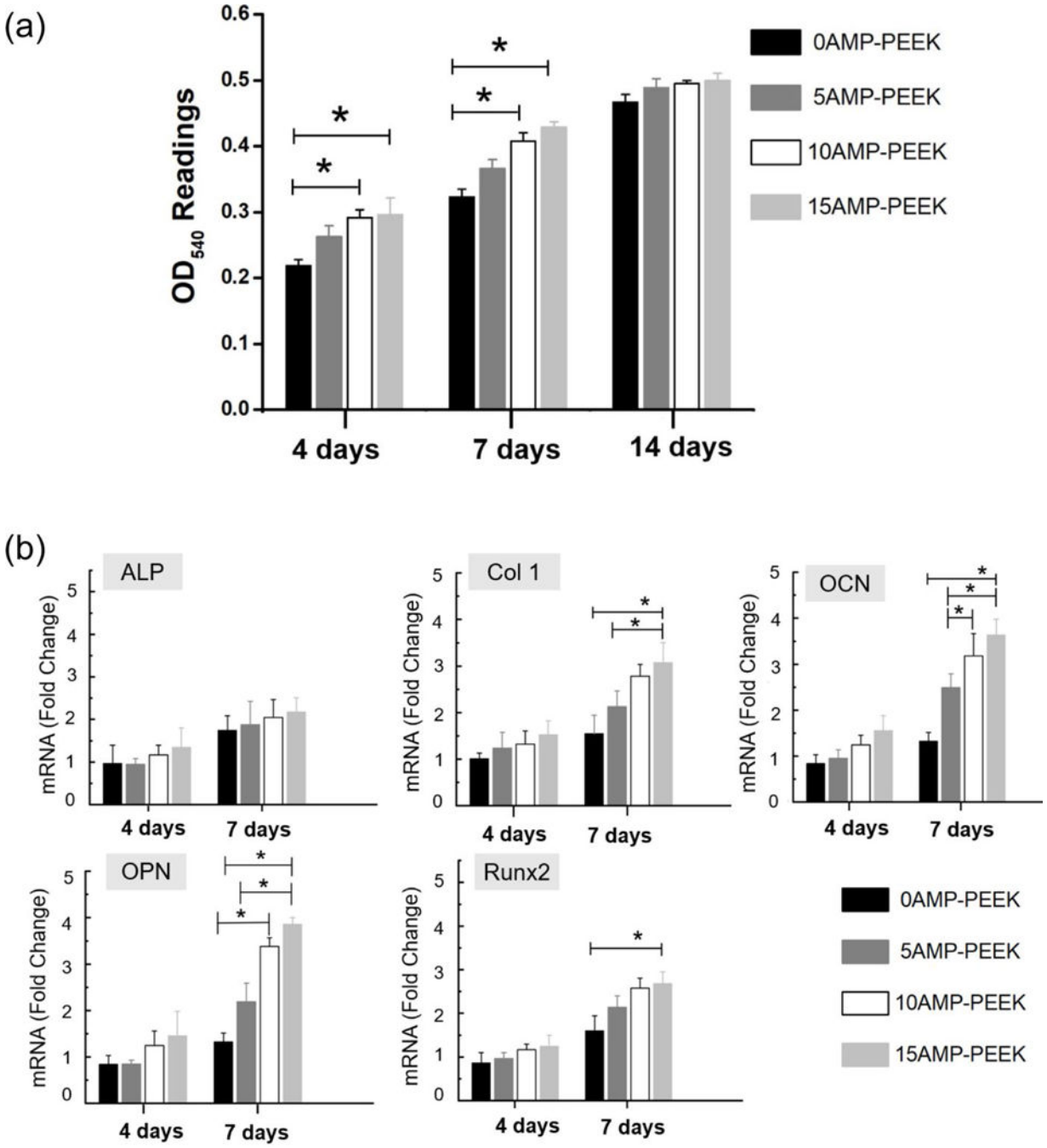

Figure 6.

In vitro results of AMP-PEEK composites. **(a)** OD_{540} readings from the MTT assay results at different time frames. Of note, is the higher proliferation of MC3T3 cells on the composites as opposed to bare PEEK. **(b)** qRT-PCR results showing mRNA expressions of different genes (as fold-change with respect to control PEEK) after 4- and 7-days culture.

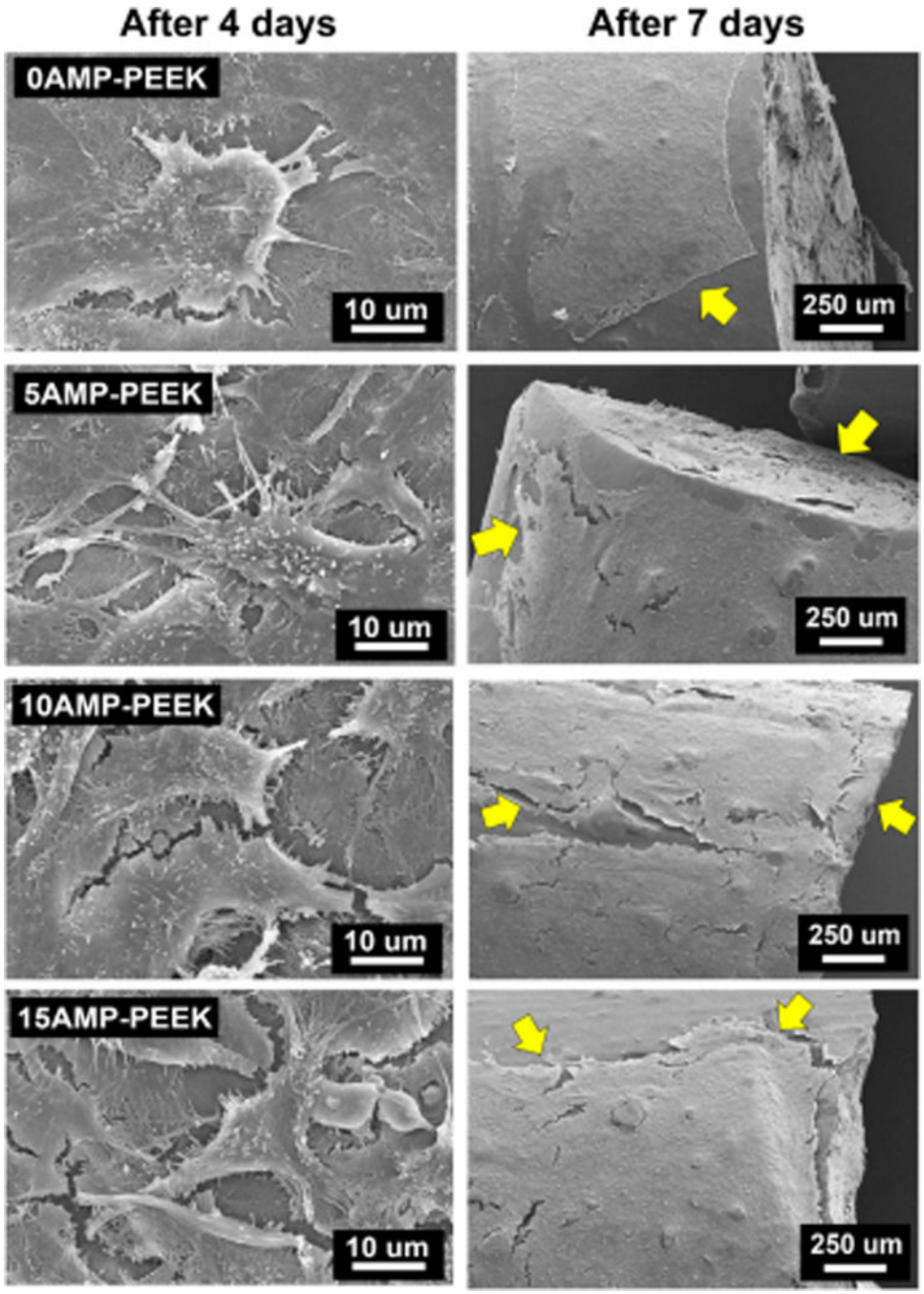

Figure 7.
SEM micrographs showing MC3T3 cell adhesion and growth on various specimens after 4 and 7 days. Of note is the flattened morphology, filopodia attachment and connection to form a sheet of cells within 7 days.

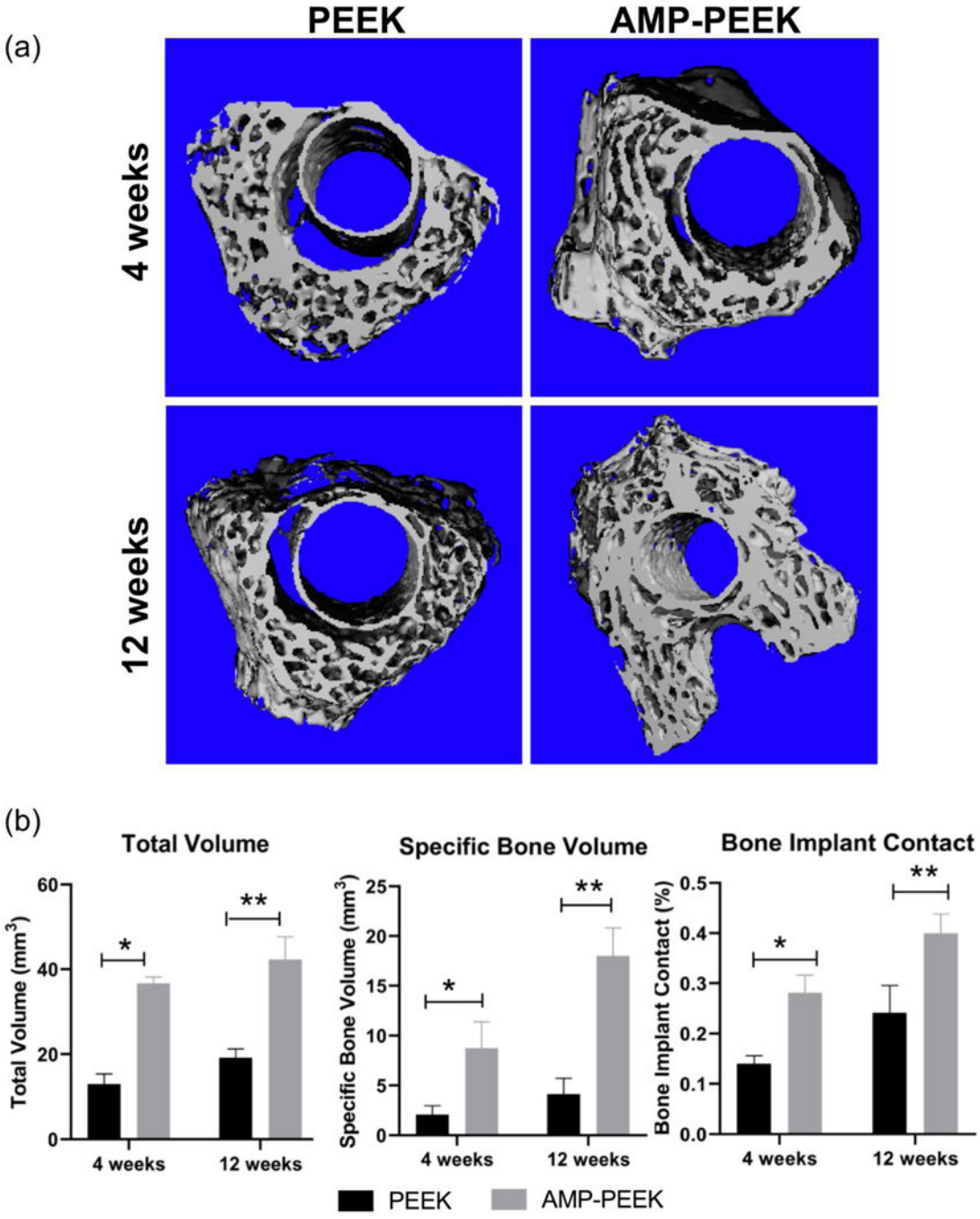

Figure 8.

(a) Representative micro-CT images showing 3-D reconstruction of the region near PEEK and AMP-PEEK implants after 4- and 12-weeks implantation. **(b)** Total volume, specific bone volume and bone-implant contact values of micro-CT analyses calculated as bone volume area and percentage of the total implant perimeter. Results are shown as area and mean percentages ± standard deviation. Various statistically significant differences are indicated by asterisk. Total Volume: * p=<0.0001; ** p=<0.0001; Specific Bone Volume: * p=<0.0001; *p= 0.0001. Bone Implant Contact: *p=0.0002; ** p=<0.0001.

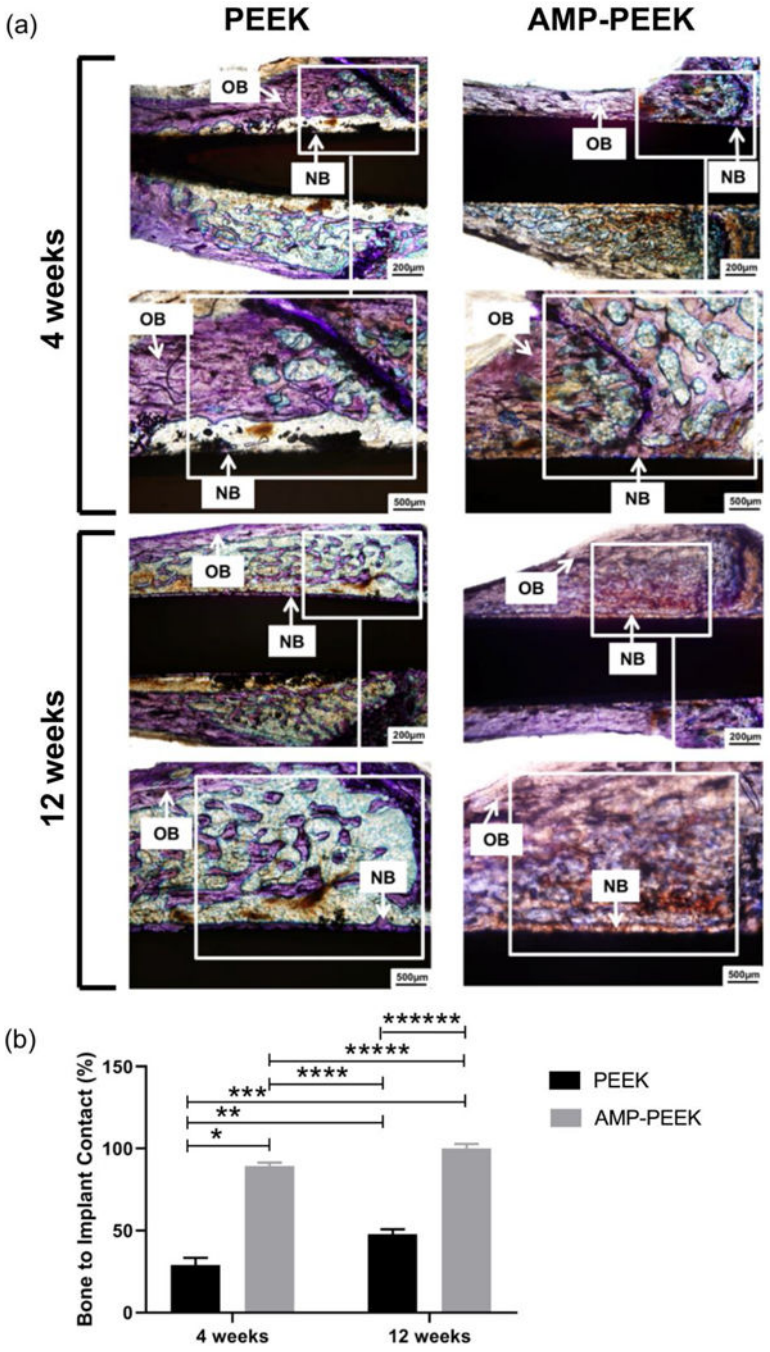

Figure 9.

(a) Representative photomicrographs of toluidine blue stained thin sections in bright field of PEEK and 15AMP-PEEK at 4 weeks and 12 weeks post-implantation. Observe the presence of more new bone formation and the contact between bone and the 15AMP-PEEK implant at both time points. Also, after 12 weeks, 15AMP-PEEK shows the formation of substantial amount of compact trabecular bone as opposed to PEEK. (OB: Old Bone and NB: New Bone) **(b)** Histomorphometric analysis of bone-to-implant contact (BIC) at 4- and 12-weeks post-implantation, calculated as a percentage of the total implant perimeter. Statistically

significant differences are indicated by an asterisk, * $p<0.0001$; ** $p=0.0026$; ***$p<0.0001$; ****$p<0.0001$; *** $p=0.1198$ and ***$p<0.0001$.

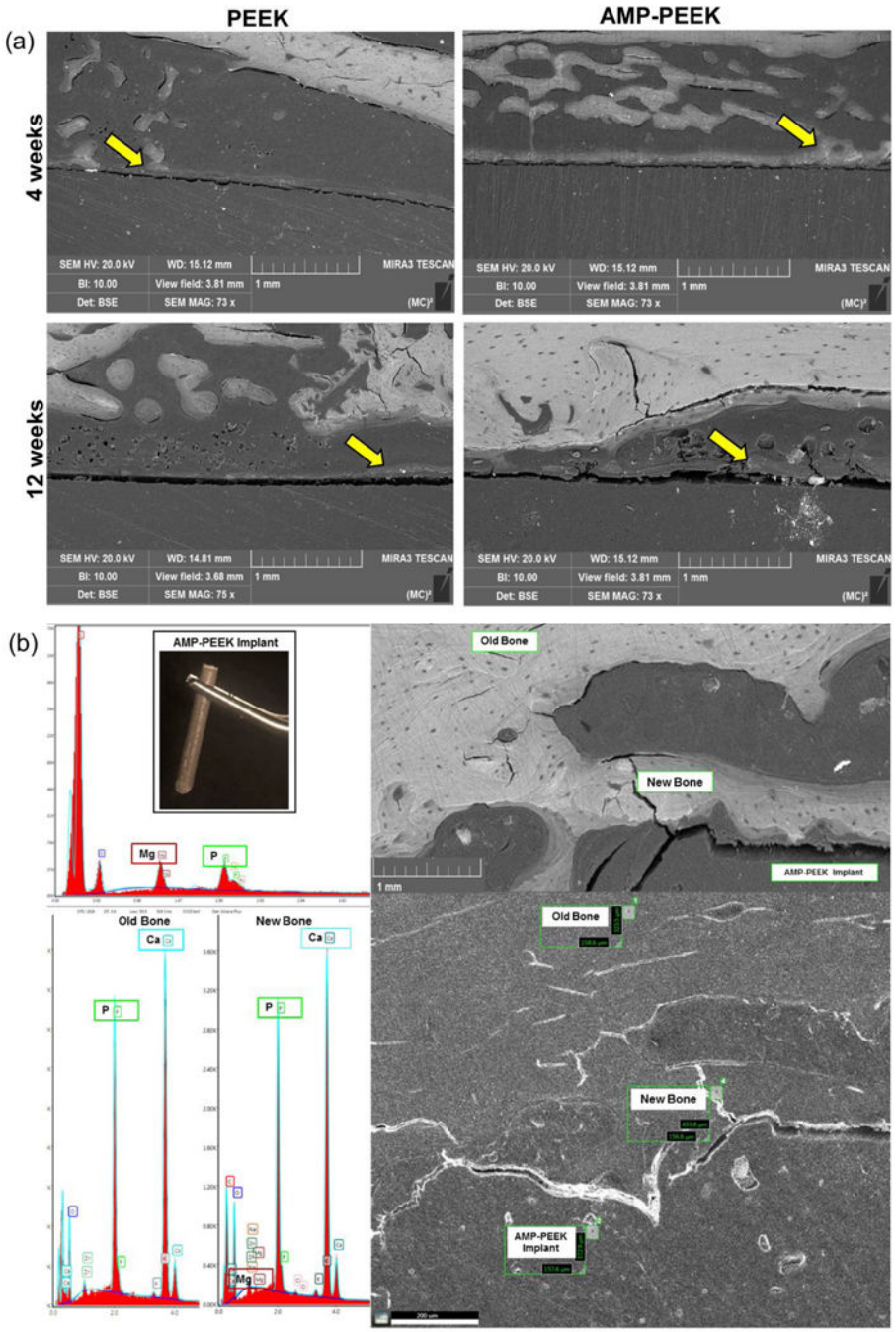

Figure 10.

(a) Backscatter SEM images of PEEK and PEEK-AMP implants at 4 weeks and 12 weeks post-implantation. Yellow arrows indicate the formation of new mineralized bone. **(b)** EDS semi-quantitative chemical composition assessment at various regions of the different samples and SEM micrograph acquired immediately after retrieval showing the presence of mineralized tissue in contact with the exposed implant's surface edges. BSE-SEM micrograph showed close contact between bone and implant for all samples.

Table 1.

Specimen name, corresponding compositions and their residence time during melt-blending.

Specimen Name	AMP vol. %	PEEK vol. %	Residence Time (mins)
0AMP-PEEK	0	100	0
5AMP-PEEK	5	95	6
10AMP-PEEK	10	90	12
15AMP-PEEK	15	85	15

Table 2.

Melting temperatures, enthalpy and percent crystallinity of specimens with varying AMP percentage. Curve fitting results of different specimens as obtained by power law model ($\eta=k\omega n-1$, Cox−Merz rule); dynamic viscosity was converted into shear viscosity and fitted in the model. *k* is the flow consistency index and *n* is the flow behavior index.

Specimen Name	Tm (°C)	Hm (J/g)	Xcw (%) - DSC	k	n
0AMP-PEEK	338.21	32.9869	25.38	8400	0.53
5AMP-PEEK	339.10	31.3710	25.67	8900	0.5
10AMP-PEEK	338.91	30.0969	26.31	10500	0.46
15AMP-PEEK	338.20	31.0460	28.76	11600	0.42
				$R^2 > 0.9$	

Table 3.

Melting temperatures, enthalpy and percent crystallinity of 10AMP-PEEK specimens processed (melt-blended) at varying temperatures.

Processing Temp	Tm (°C)	Hm (J/g)	Xcw (%) - DSC
360 °C	338.75	27.6236	24.14
370 °C	337.84	30.0969	26.31
380 °C	337.43	30.1023	26.31
400 °C	337.18	30.2043	26.40